Supplemental Information

INVENTORY OF SUPPLEMENTAL INFORMATION

Supplemental Figures

Supplemental Tables

Extended Experimental Procedures

Supplemental References

SUPPLEMENTAL FIGURES

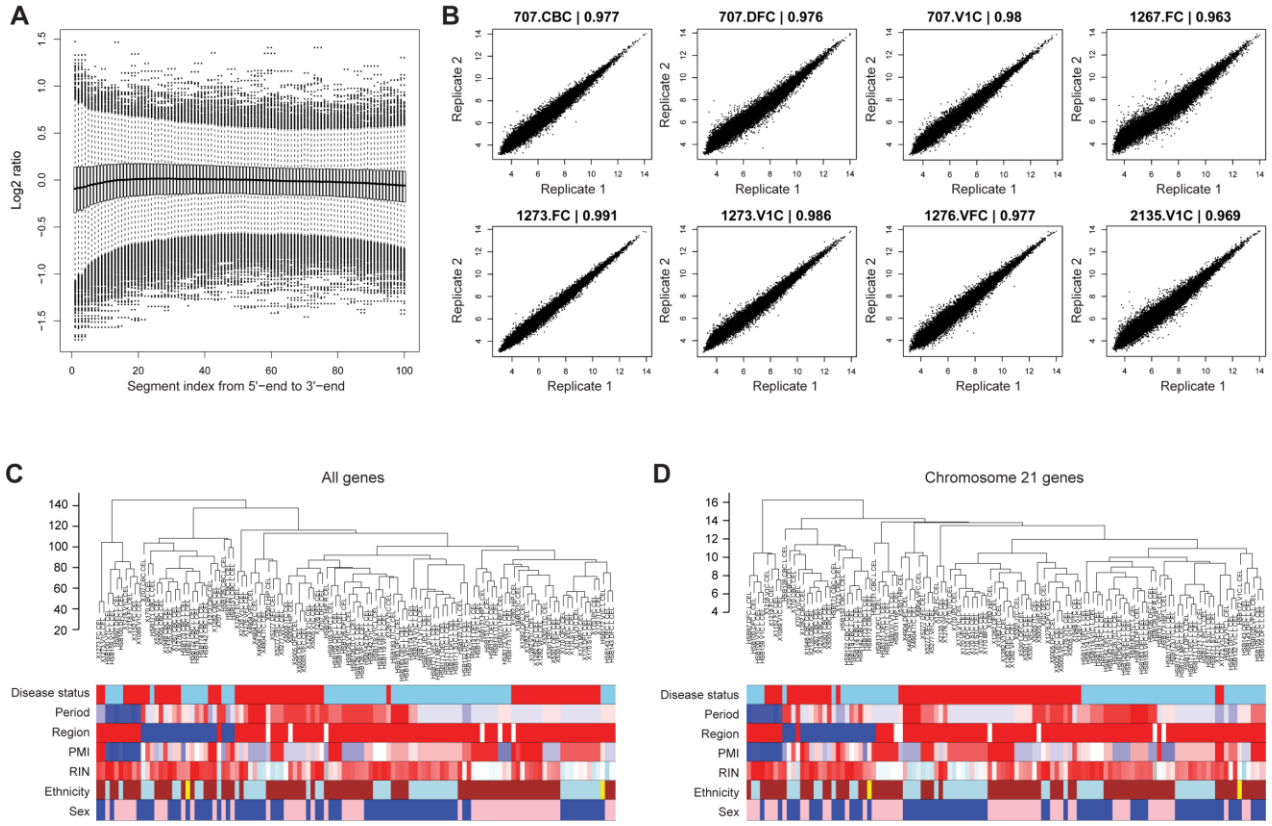

Figure S1. Robustness and Reproducibility of the Exon Microarray Protocol. Related to Figure 1

(A) Box plots showing the log2 intensity of 100 segments divided along the longest transcript of each gene from the 5'-end to 3'-end compared to the expression of the whole gene indicating array hybridization uniformity.

(B) Spearman correlation analysis of eight samples, which were re-tested to confirm technical reproducibility.

(C-D) Hierarchical clustering of all genes (C) or chromosome 21 (HSA21) genes (D) indicating genes cluster most strongly according to region and developmental period rather than disease status or other factors. Disease status (light blue, euploid control; red, Down syndrome), period (blue to red representing younger to old), region (blue, neocortex [NCX; all neocortical areas/regions combined]; white, hippocampus [HIP]; red, cerebellar cortex [CBC]), postmortem interval (PMI; low to high representing blue to red), RNA integrity number (RIN; low to high representing blue to red), ethnicity (African-American, light blue; Caucasian, brown; Hispanic, yellow), and sex (blue, male; pink, female).

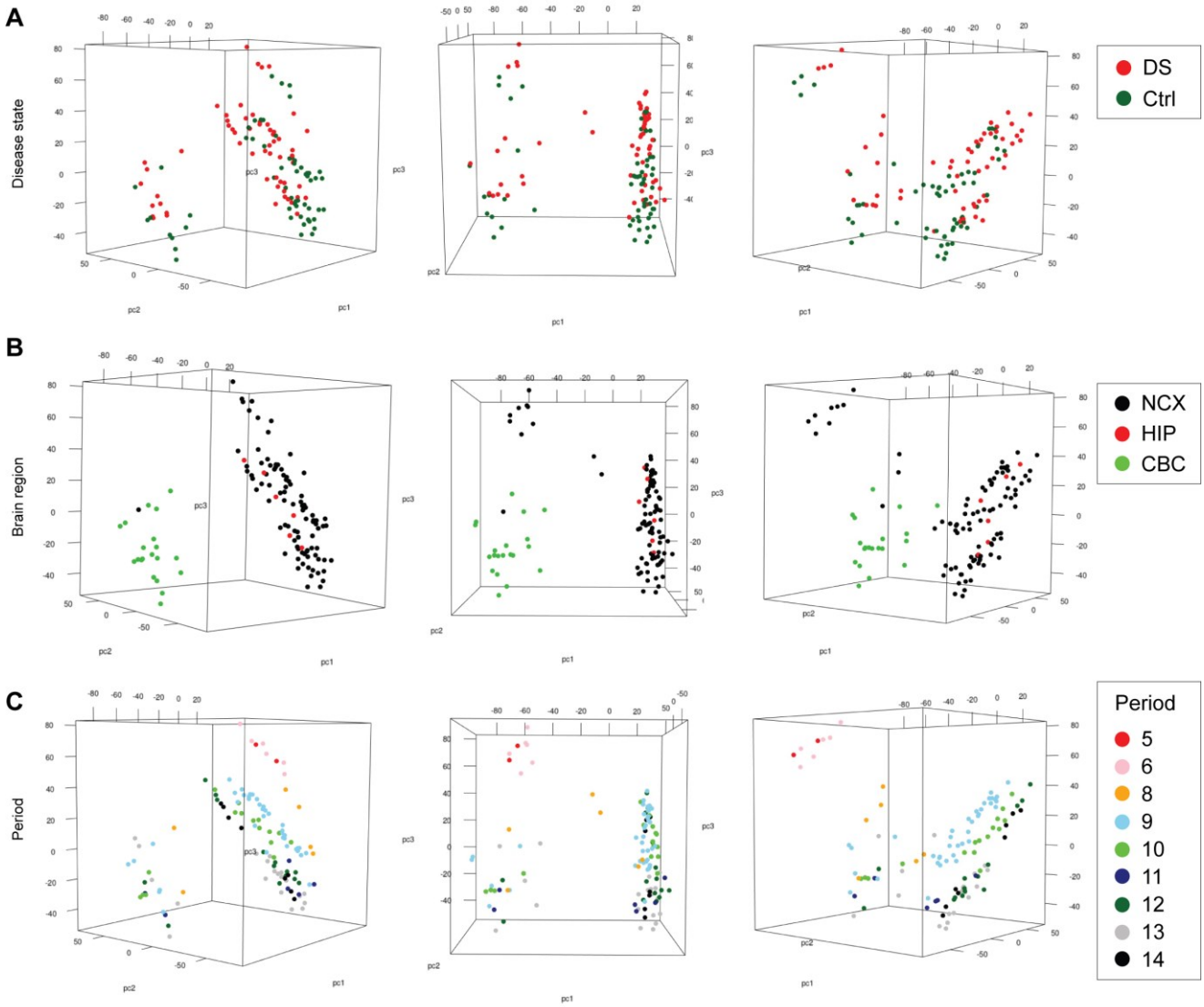

Figure S2. Principle Component Analysis Reveals that Brain Region and Age Contribute More to Transcriptional Differences than Disease Status. Related to Figure 1

(A)Three-dimensional plots of the principle component analysis (PCA) of Down syndrome (DS) samples and their matched euploid controls (Ctrl) rotated in 3 different views for better visualization and colored according to disease status. Note fairly minimal differences between DS versus Ctrl clusters.

(B) Three-dimensional plots of the PCA of DS samples and their matched controls rotated in 3 different views for better visualization and colored according to brain region (NCX [pooled neocortical regions/areas], HIP, and CBC). Note the large separation of CBC clusters from NCX and HIP.

(C) Three-dimensional plots of the PCA of DS and Ctrl samples rotated in 3 different views for better visualization and colored according to developmental period. Note that there are clear patterns defining distinct developmental periods, that display larger separation than disease state, but more moderate separation than CBC versus NCX/HIP clusters.

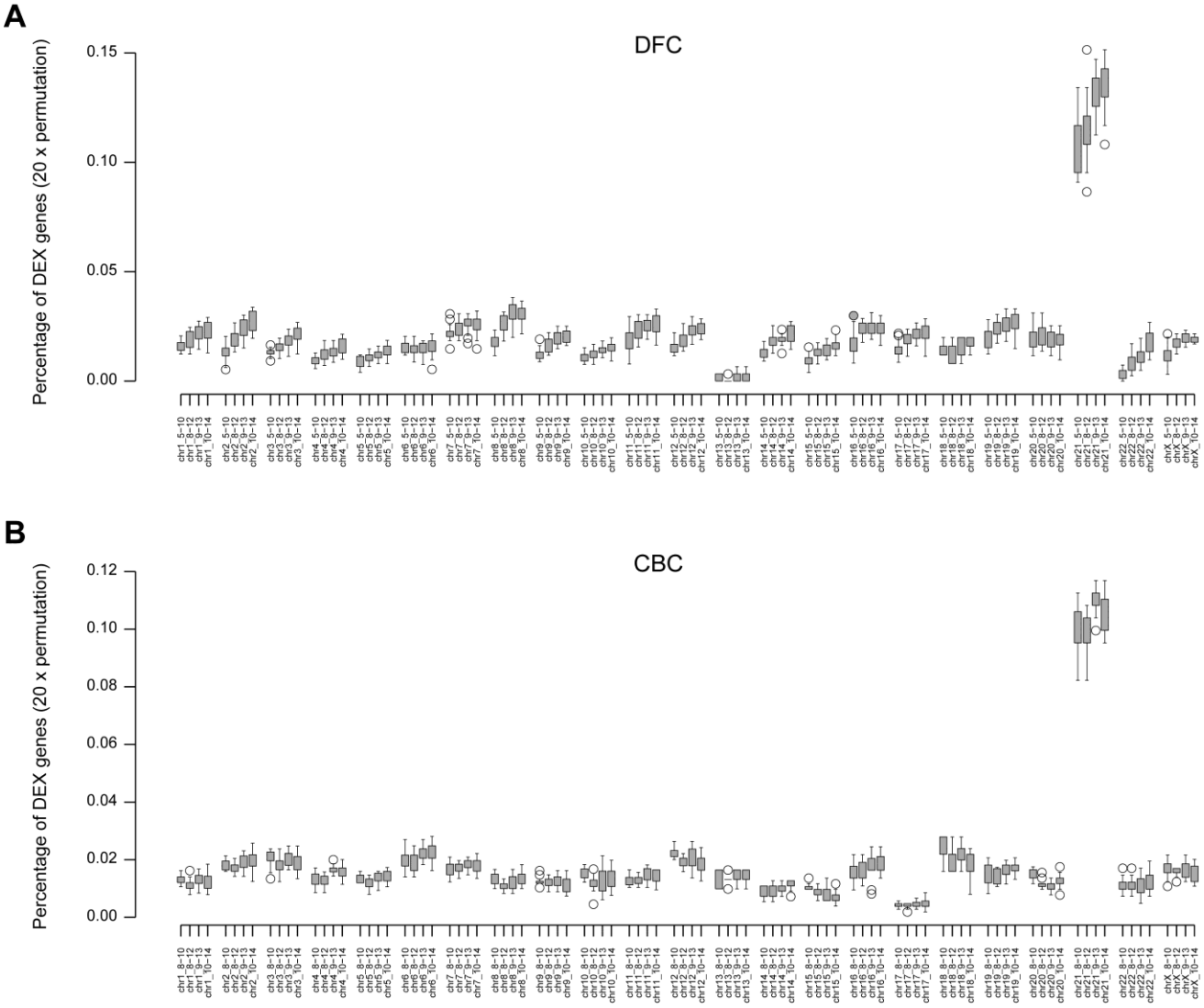

Figure S3. Developmental Dynamics in the Proportion of Dysregulated Genes Across Chromosomes. Related to Figure 1

(A and B) The distribution of differentially expressed (DEX) genes percentages in each chromosome across four sliding window periods calculated from 20 cycle permutations for the dorsolateral prefrontal cortex (DFC) (A) and CBC (B). The percentage of DFC expression rose across the sliding window periods in nearly all chromosomes, while the developmental dynamics in the proportion of DEX genes was variable between chromosomes in the CBC, with most chromosomes exhibiting no change in the percentage of DEX genes across development. For the permutation test, DS samples were randomly matched to control samples within the same stage and with the same sex to identify DEX genes.

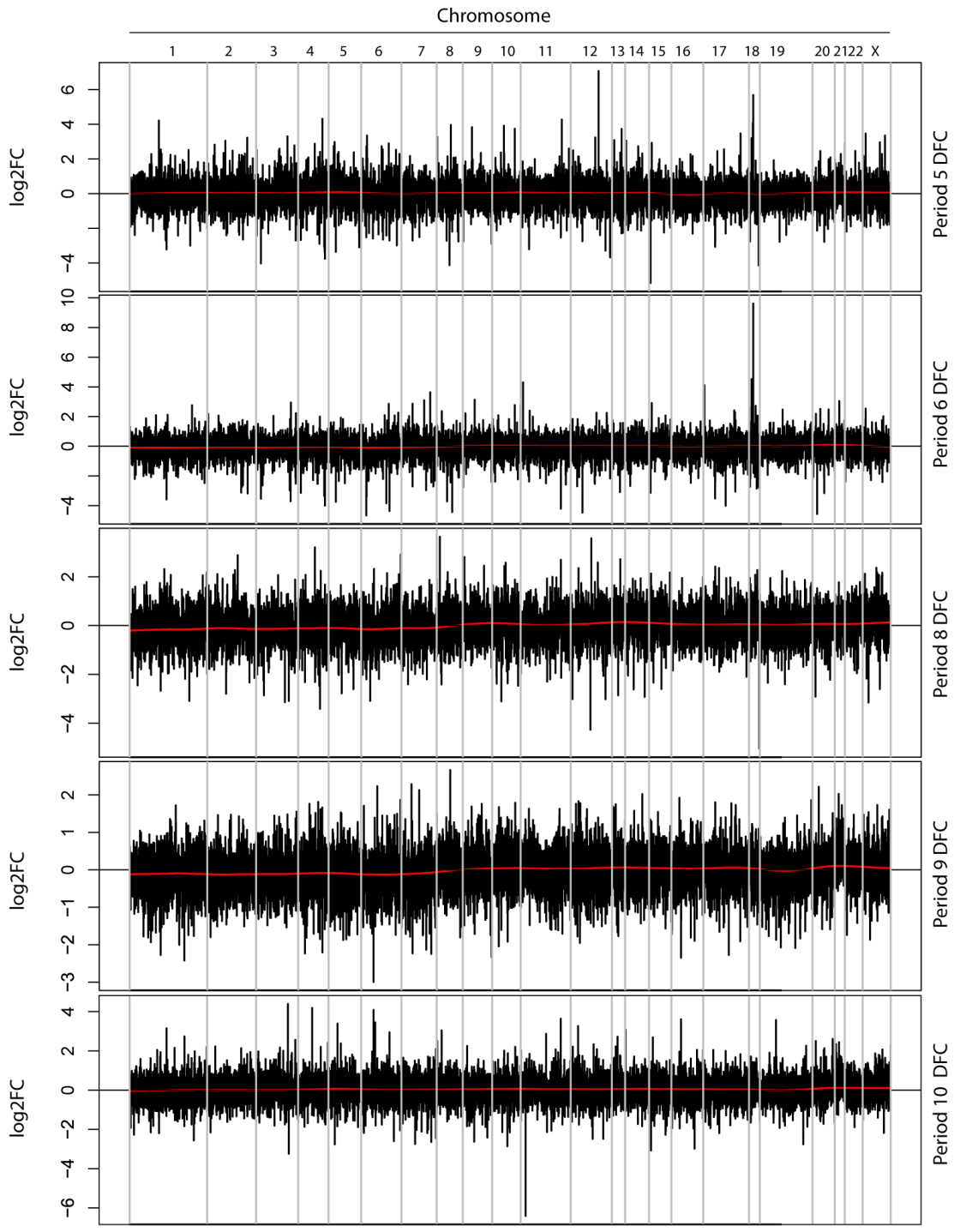

Figure S4. Gene Expression Fold Change is Not Organized in Chromosomal Domains in the Down Syndrome Brain Transcriptome. Related to Figure 1

Representative plots of a period-specific genome-wide expression variations (log2 fold change [log2FC]) for the DFC indicate a lack of widespread and contiguous genomic regions of up-regulated or down-regulated gene expression in DS brain. A LOWESS smoothing function (red trace) demonstrates minimal deviation from zero.

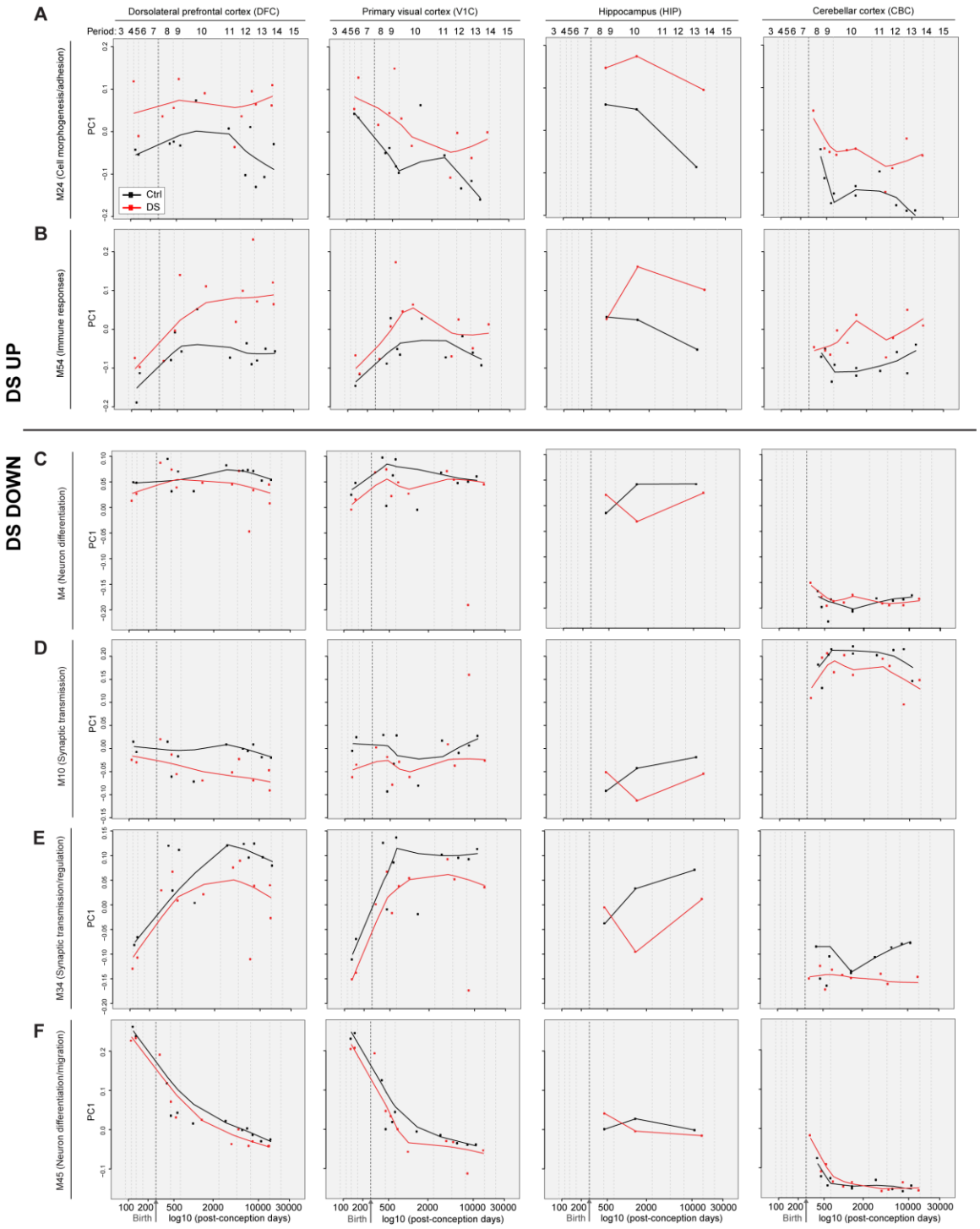

Figure S5. Representative Co-Expression Modules with Differential Expression in Down syndrome Brains. Related to Figure 2

(A) Plots of relative expression of the principal component 1 (PC1) of gene co-expression module (M) 24 over development in the DFC, primary visual cortex (V1C), HIP, and CBC, indicating higher expression in DS versus control forebrain that increases over development. Subsequent gene ontology analysis revealed that this module was enriched in genes associated with cell morphogenesis/adhesion.

(B) Plots of relative expression of the PC1 of M54 over development in the DFC, V1C, HIP, and CBC, indicating higher expression in DS versus control forebrain that increases over development. Subsequent gene ontology analysis revealed that this module was enriched in genes associated with immune responses.
(C) Plots of relative expression of the PC1 of M4 over development in the DFC, V1C, HIP, and CBC, indicating decreased expression in DS versus Ctrl brain over development. Subsequent gene ontology analysis revealed that this module was enriched in genes associated with neuron differentiation.
(D) Plots of relative expression of the PC1 of M10 over development in the DFC, V1C, HIP, and CBC, indicating decreased expression in DS versus Ctrl brain over development. Subsequent gene ontology analysis revealed that this module was enriched in genes associated with synaptic transmission.
(E) Plots of relative expression of the PC1 of M34 over development in the DFC, V1C, HIP, and CBC, indicating decreased expression in DS versus Ctrl brain over development. Subsequent gene ontology analysis revealed that this module was enriched in genes associated with synaptic transmission/regulation.
(F) Plots of relative expression of the PC1 of M45 over development in the DFC, V1C, HIP, and CBC, indicating decreased expression in DS versus Ctrl brain over development. Subsequent gene ontology analysis revealed that this module was enriched in genes associated with neuron differentiation.

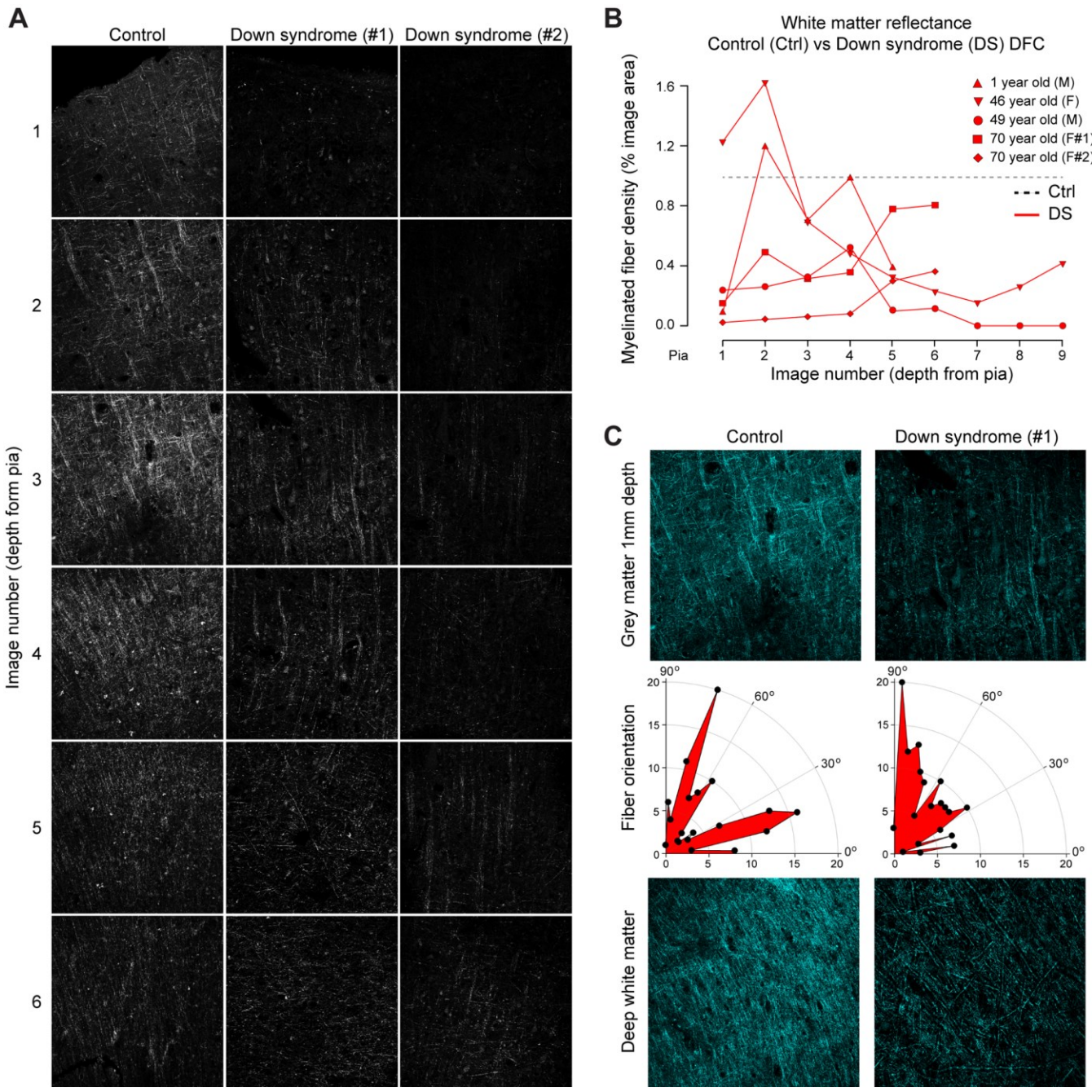

Figure S6. Myelin Laser Reflectance Signatures are Reduced in Down Syndrome Neocortex. Related to Figure 3 and Figure 7

(A) Spectral confocal reflectance microscopy of 70 year old Ctrl and DS tissue sections of the DFC.

(B) Quantification of myelinated fiber density neocortical images from five DS cases captured from the pial surface down to the compacted white matter. Each brain is compared to its respective control brain (black line).

(C) Representative examples of myelinated fiber orientations at two different depths within 70 year old Ctrl and DS brains. Polar plots depict the fiber orientations.

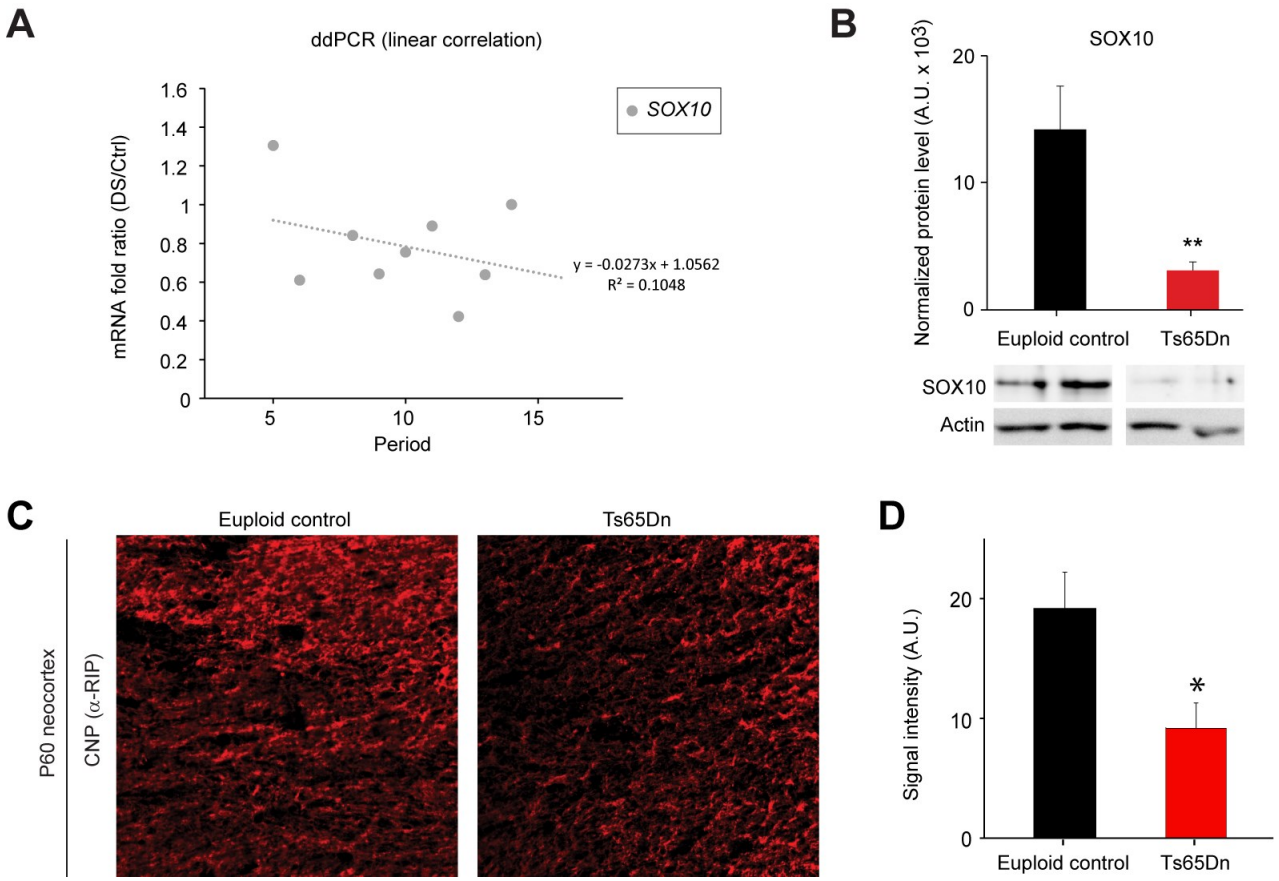

Figure S7. Oligodendrocyte-Related Genes and Proteins are Reduced in Down Syndrome and Ts65Dn Mouse Neocortex. Related to Figures 3 and 7

(A) ddPCR analysis of human euploid Ctrl and DS DFC shows down-regulation of *SOX10* expression in developing and adult DS brain.

(B) Western blot measurements of SOX10 protein levels in the Ctrl and Ts65Dn mouse corpus callosum (CC) at P30. **, $p<0.03$ (paired t-test).

(C) Representative immunofluorescence labeling of the corpus callosum in P60 euploid Ctrl and Ts65Dn mice using the RIP antibody raised against CNP.

(D) Quantitative analysis of the intensity of RIP immunostaining reveals a significant decrease in Ts65Dn compared to euploid Ctrl mice. *, $p<0.02$ (paired t-test).

SUPPLEMENTAL TABLES

Table S1. Demographic, clinical, and tissue quality details for all samples. Related to Figure 1.

Table S2. Descriptions of anatomical regions analyzed. Related to Figure 1, 3, and S6.

Table S3. DEX genes on each chromosome. Related to Figure to Figure 1.

Table S4. DEX genes across the sliding window periods. Related to Figure 1, 3, and 5.

Table S5. GO analysis of DEX genes. Related to Figures 1 and 2.

Table S6. List of WGCNA modules and GO categories. Related to Figures 2, 7, and S5.

Table S7. List of genes within each WGCNA module. Related to Figures 2, 7, and S5.

Table S8. Expression analysis of cell type-specific marker genes across tissues. Related to Figures 2 and 7.

Table S9. Lists of OPC and OL enriched genes highly co-expressed in the developing human brain. Related to Figure 7.

EXTENDED EXPERIMENTAL PROCEDURES

Human Tissue

This study was conducted using postmortem human brain specimens from tissue collections at the Department of Neuroscience, Yale School of Medicine, and the University of Maryland Brain and Tissue Bank (Baltimore, MD), Brigham and Women's Hospital Pathology Department, and Boston University Pathology Department. Tissue was collected after obtaining parental or next of kin consent and with approval by the institutional review boards. Tissue was handled in accordance with ethical guidelines and regulations for the research use of human brain tissue set forth by the NIH (http://bioethics.od.nih.gov/humantissue.html) and the WMA Declaration of Helsinki (http://www.wma.net/en/30publications/10policies/b3/index.html).

Appropriate informed consent was obtained and all available non-identifying information was recorded for each specimen. Specimens ranged in age from 14 post-conception week (pcw) to 40 years. The postmortem interval (PMI) was defined as hours between time of death and time when tissue samples were frozen (Table S1).

Human Tissue Dissection and Neuropathological Evaluation

All clinical histories, tissue specimens, and histological sections were evaluated to assess for hypoxia, cerebrovascular incidents, tumors, microbial infections, neurodegeneration, demyelination, and metabolic disease.

Trisomy 21 was confirmed by karyotyping and/or Illumina Omni-2.5 million SNP arrays. The localization of dissected samples was verified by histology in the postnatal brains and across fetal periods using the same anatomical landmarks. The complete list of periods and samples, including corresponding putative functional brain regions and neocortical areas, analyzed in this study can be found in Table S1, S2A and S2B.

Fresh frozen postmortem brain specimens from donors affected with DS and from neurotypical euploid controls matched on age and sex (see Tables S1 and S2 for the list of brain specimens, tissue samples and brain regions analyzed) were dissected as follows. For fetal brains, the entire neocortical plate and adjacent superficial part of the subplate zone was sampled; for postnatal brains the entire thickness of the cortex, containing all six cortical layers, and the underlying gyral white matter corresponding approximately to white matter segment 4 as defined by von Monakow were sampled. Hippocampal samples were dissected from the middle third of the hippocampus proper. Samples of the cerebellar cortex were dissected from lateral part of posterior lobe of cerebellum and they contain all three layers of cerebellar cortex and underlying white matter, but do not contain cerebellar nuclei. Tissue dissection was done using a dental drill (AnyXing, 300D) with a Lindemann Bone Cutter H162A.11.016 and diamond disk saw (Dental Burs USA; r=11 mm) on an aluminum plate over dry ice.

To prepare tissue sections for microscopic histological and neuropathological examination, small samples (usually the dorsal parietal cortex, striatum with ependymal layer, hippocampus, and the cerebellum) were dissected and fixed in 4% paraformaldehyde and processed for histology and immunohistochemistry as described below. Neocortical cytoarchitecture of each euploid control sample was compared to areal cytoarchitectonic maps to distinguish Brodmann areas (BA). Euploid control specimens with incorrect cytoarchitecture or abnormal microscopical appearance were excluded from the study. Neocortical areas (see below) were grouped according to the lobes from which they were sampled. The same anatomical landmarks were used to dissect DS brain specimens.

Frontal lobe

Dorsolateral prefrontal cortex (DFC) was sampled from approximate border between the anterior and middle third of the medial frontal gyrus. Cytoarchitectonically, DFC corresponds approximately to Brodmann area (BA) 9 and BA46.
Orbital prefrontal cortex (OFC) was sampled from the anterolateral two thirds of the orbital gyri. OFC corresponds approximately to BA11.
Ventrolateral prefrontal cortex (VFC) was sampled from the posterior third of the inferior frontal gyrus, corresponding to the opercular and triangular part of the inferior frontal gyrus. VFC corresponds approximately to BA44 and BA45.
Medial prefrontal cortex (MFC) was sampled from perigenual and subgenual parts of the anterior cingulate gyrus and the anteromedial part of the superior frontal gyrus. MFC corresponds approximately to BA24, BA32 and BA33.

Parietal lobe
Primary somatosensory cortex (S1C) was sampled from the ventrolateral part of the postcentral gyrus adjacent to the M1C area. S1C corresponds to BA1, BA2 and BA3.
Posterior inferior parietal cortex (IPC) was sampled from the posterior half of the supramarginal gyrus. IPC corresponds approximately to BA40.

Temporal lobe
Posterior superior temporal cortex (STC) was sampled from the posterior third of the superior temporal gyrus. STC corresponds approximately to BA22.
Inferior temporal cortex (ITC) was sampled from the anterior third of the inferior temporal gyrus. ITC corresponds approximately to BA20.

Occipital lobe
Primary visual cortex (V1C) was sampled from the area surrounding the calcarine fissure. Only samples in which the stria of Gennari could be recognized were included. V1C corresponds to BA17. Small pieces of the neighboring BA18 could have been occasionally present in the sample, but the majority of the sample corresponded to BA17.

Hippocampus (HIP) was sampled from the middle third of the retrocommissural hippocampal formation, located on the medial side of the temporal lobe. Sampled areas always contained dentate gyrus and the cornu ammonis. Samples dissected from the frozen tissue may contain small quantities of the neighboring choroid plexus.

Cerebellar cortex (CBC) was sampled from the lateral part of the posterior lobe. The sampled area contained all three layers of cerebellar cortex and underlying white matter but not the deep cerebellar nuclei. CBC approximately corresponds to the lateral pontocerebellum.

Spectral Confocal Reflectance Microscopy
Spectral confocal reflectance microscopy (SCoRe) (Schain et al., 2014) was used to quantify myelinated axon segments in tissue sections of the DFC dissected from 4% paraformaldehyde fixed brains. We analyzed tissue from five pairs of matched brains obtained from the University of Maryland Brain and Tissue Bank, Brigham and Women's Hospital Pathology Department and Boston University Pathology Department: one pair from 1 year old brains, one pair of 46 year old brains, one pair of 49-50 year-old brains and two pairs of 70 year old brains. Tissue sections for the 46-50 year old cases were 4μm paraffin sections from Pathology collections at Boston University and Brigham and Women's Hospital whereas all other cases were 100μm vibratome-cut formalin-fixed sections from the Maryland Brain Bank. We found that SCoRe microscopy parameters did not vary between sections based on how thick they were or how they were processed prior to microscopy. Each pair constituted an experiment and the laser power and detector sensitivity settings were calibrated first to the euploid

control brain section to yield a thresholded image highlighting the myelinated axon segments within the image. The same imaging settings were then used for the Ts21 brain of that pair. Images (1024 x 1024; 425 mm x 42 5mm) were collected using reflectance from 488nm, 561nm and 633nm laser lines collected with 486-501 nm, 554-563 nm and 630-634 nm filters respectively using a 20X, 0.8NA objective lens. For each brain, we collected overlapping SCoRe images from the DFC in a radial stripe from the pial surface down to the compacted white matter underneath the cortical grey matter. We calculated the myelinated fiber density within each image as the percent of the image pixels containing a myelin reflectance signal.

RNA Isolation and Exon Array Hybridization

Total RNA was isolated from 30mg of pulverized frozen brain tissues using a non-phenolic procedure (RNeasy Plus Mini Kit, Qiagen), followed by DNase treatment (TURBO DNase, Ambion). Optical density values at 260/280 were consistently above 1.9 (NanoDrop, Thermo Scientific), and samples with RNA integrity values of at least 5 were used for microarray (RIN>5, Agilent Bioanalyzer). Synthesized cDNA (5.5 µg) using WT Expression kit (Ambion) was labeled and loaded onto individual Affymetrix Human Exon 1.0 ST arrays. Microarrays were hybridized at 45 °C for 16–24 hours, washed and stained using an Affymetrix FS450 fluidics station, according to manufacturer recommendations. Microarrays were scanned on a GeneChip Scanner 3000 and visually inspected for hybridization artifacts. Exon chip analysis was performed using Affymetrix Power Tools 1.12.0. Probe level data was summarized into probe set level data using the Robust Multichip Average (RMA) background correction algorithm in combination with an R-script. The raw image files (.DAT files) were analyzed using Affymetrix GeneChip Operating Software to generate .CEL files.

Quality Control Measures

Three QC measures were performed to test the quality of exon array data. First, ratio intensity plots were plotted for all exon arrays to detect spatial artifacts that are defined as severe non-random spatial patterns of exon arrays. The construction of these ratio intensity plots was previously described (Kang et al., 2011). Second, exon array hybridization uniformity was estimated by gene expression uniformity from 5'-end to 3'-end (Figure S1A). Microarrays displaying spatial artifacts and altered hybridization uniformity were excluded for further data analysis. Third, 8 samples were re-tested to evaluate technical reproducibility (Figure S1B). The correlations were high for these technical replicates (Spearman correlation, r2 = 0.977; N=16, Figure S1B).

Data Normalization

Affymetrix exon array raw data (.CEL files) were normalized using the Partek Genomics Suite version 6.6 to generate probeset-level (exon-level) and transcript cluster (gene-level) intensities. The expression level of a probe set was estimated by averaging the intensities of all core probe sets within the exon. We applied the following default Partek settings: RMA background correction, exclusion of probes containing SNPs, quantile normalization, mean probe set summarization, and log2-transformation. Only core probe sets defined by Affymetrix were included for the calculation. These core probe sets have reliable sequence annotations. The expression level of a gene (transcript cluster) was estimated using the median of all exons within the gene.

Transcriptome Data Analyses

Principal component analysis was applied to visualize the relatedness of DS and their-matched control samples. The first three principal components were calculated using the function “prcomp” in R. All these principal components were plotted using the function “plot3d” in R. Each data point in the picture represents one sample. All samples were colored according to the phenotype of the samples, such as brain region, period, and disease status (Figure S2). To make these pictures clearer, three different directional views are displayed.

A paired t-test was used to identify DEX genes between paired DS and matched control samples across all development periods. FDR-adjusted p-value < 0.1 was used as a cutoff. To see how the DEX genes distribute along the human genome, chromosome location of these DEX genes were determined based on the gene annotations provided by Affymetrix. Chromosomes 1 to 22, X and Y were investigated. The percentage of DEX genes and ratio of up-regulated/down-regulated genes in each chromosome were calculated.

To identify differentially expressed (DEX) genes between paired DS and matched control tissue samples at specific developmental periods, a sliding-window approach and paired t-test were used. The window size was set to 3 periods. For each window, a paired t-test was applied to determine if the expression level of a gene in DS brain samples was significantly different from the expression level in the samples from the matched control. Statistical threshold was set at a p-value < 0.05 and minimum fold difference > 2 between DS and control brains. We performed a 20-cycle permutation test to ensure that our results are robust and are not unduly influenced by any particular sample. For the permutation test, DS samples were randomly matched to control samples within the same stage and with the same sex to identify DEX genes using the same approach and cutoff. The distributions of the number of DEX genes from different match sets were plotted in a boxplot.

Unsupervised signed co-expression networks were constructed using the weighted gene co-expression network analysis (WGCNA) package in R (Zhang and Horvath, 2005). All genes with core probe sets were included in the analysis. A pair-wise correlation matrix was computed, and an adjacency matrix was calculated by raising the correlation matrix to a power. The power was set to 21 according to a scale-free topology criterion (Zhang and Horvath, 2005). For each pair of genes, a robust measure of network interconnectedness (topological overlap measure) was calculated based on the adjacency matrix. The topological overlap based dissimilarity was then used as input for average linkage hierarchical clustering. Modules were generated by hybrid dynamic tree-cutting. To obtain co-expression patterns, we set the minimum module size to 20 genes, deepSplit to 2, and the minimum height for merging modules to 0.15. Each module was summarized by an eigengene, which is the first principal component of the scaled module expression. To obtain cleaner modules, we defined the module membership measure (also known as module eigengene based connectivity kME) as the correlation between gene expression values and the module eigengene. Genes were iteratively assigned to the module with highest kME as long as they had maximum kME > 0.7. The module membership is also used to rank genes in the module. Top ten genes in the rank were considered as hub genes of module.

For differential expressed genes and co-expression modules, functional enrichment was assessed using the DAVID Bioinformatics Resource 6.7 (http://david.abcc.ncifcrf.gov/).

Analysis of Oligodendrocyte Precursor Cells and Oligodendrocyte Associated Gene Expression

To identify the cell type expression profile of all 121 genes expressed in module (M) 43 (the myelination associated module in Figure 2), we determined if they were highly expressed (FPKM > 20) in acutely purified representative populations of neurons, astrocytes, oligodendrocyte precursor cells (OPCs), newly formed oligodendrocytes, myelinating oligodendrocytes (mOLs), microglia, endothelial cells, and pericytes from mouse cerebral cortex at postnatal day 7 (see Zhang et al. 2014; http://web.stanford.edu/group/barres_lab/brain_rnaseq.html).

Furthermore, to identify genes that are specifically expressed in OPCs and mOLs (Figure 7), but not other cell types, during fetal and early postnatal human brain development we generated a set of genes that were found to both be highly enriched in OPCs and mOLs using the mouse dataset (Zhang et al. 2014) and in a list of OL and OPC related human genes generated in our previous study that categorizes genes according to their correlations with major cell types and neurodevelopmental processes across human development (Kang et al., 2011). By overlapping these two lists allowed us to create a set of human homologs that are most likely to be selectively enriched in OPCs and mOLs during human fetal and postnatal development. Note that the list in Zhang et al. (2014) specifically tested purified OPCs and mOLs in mouse at one postnatal stage of development. Because OPCs are

highly proliferative at this age, the OPC list may contain genes broadly associated with cell proliferation and progenitor states. Therefore, genes that overlap between the datasets in Zhang et al. and Kang et al. provide a highly stringent set of OPC and mOL specific genes that are dynamically expressed over human development (Table S7).

The following methodology was used to derive the lists of genes highly enriched in OPCs and mOLs. The raw RPKM values from Zhang et al. (2014) were first normalized using quantile normalization. Genes enriched in mouse OPC or mOL were identified by the criterion that the fold change of each gene in these respective cell types must be 2 fold greater than in any other cell type (cell types other than OPC, newly formed oligodendrocytes and mOL). These lists were then intersected with the lists of genes highly co-expressed with OPC or mOL markers during human brain development (Kang et al., 2011) to form lists of OPC and mOL genes (Table S7). To test changes in OPC and mOL genes, paired t-test were performed between DS and control for each human developmental period. Enrichment of OPC and mOL genes in each module was calculated using Fisher's exact test (Figures 7B and 7D).

Expression Analysis of Cell Type-Specific Marker Genes Across Tissues

To confirm the accuracy and reproducibility of our dissection technique within each brain and across individuals, we determined if there was high correlation of the expression of genes enriched in neural cell types between each neocortical region across individual brains, and between samples of DFC and CBC (the brain regions for which the most tissue samples were available) from both control and DS individuals. All analyses were done using adult samples, to avoid discrepancies in developmental age that may confound pair-wise analysis. The lists of cell-type enriched genes were obtained from publically available RNA-seq data from purified astrocytes, neurons, and myelinating oligodendrocytes of the mouse cerebral cortex generated by Zhang et al. (2014). For each cell type, genes were ranked by their fold of enrichment (the fold change between this cell type and the maximum expression in the rest of cell types). Human homologs of the top 100 most enriched genes were then defined as cell-type enriched genes. Using the resulting lists of cell-type enriched genes, we calculated the Pearson correlation coefficient of oligodendrocyte, astrocyte, and neuronal human genes between samples of each neocortical area dissected from the same individual brain. If the dissection technique was consistent, high correlation should be observed as the glia/neuron ratio is more consistent throughout the neocortex than between different brain regions (Herculano-Houzel, 2014). In addition, we calculated the Pearson correlation through pairwise comparisons between samples from the CBC and DFC both within and between experimental groups (i.e., control vs control, DS versus DS, and control versus DS) for astrocytes, neurons, and oligodendrocytes. Note the limited number of samples from other brain regions precluded reliable pairwise analysis. To determine statistically significant differences in the pairwise correlation between each cell type across the experimental groups (e.g. oligodendrocyte versus astrocyte genes in DFC of paired control versus a matched control sample, matched DS versus control, and so on), we used the Wilcoxon signed-rank test (Table S8).

Droplet Digital PCR

An aliquot of the total RNA that was previously extracted from each brain region was used for secondary validation by droplet digital PCR analysis. One µg of total RNA was used for cDNA synthesis using oligo dT primers and SuperScript III First-strand synthesis Supermix (Invitrogen), and subsequently diluted with nuclease-free water to 1 ng/µl cDNA. FAM- or VIC-labeled TaqMan® probes were used for detecting copy number of target genes (Applied Biosystems). PCR reactions were conducted on the QX100 Droplet DigitalTM PCR system (Bio-Rad) according to manufacturer recommendations. The reaction mixture containing sample cDNA, primers and probe was partitioned into about 20,000 droplets in oil through the QX100 Droplet Generator. After PCR amplification (95'C 10 min; 40 cycles of (94'C 30 sec, 57'C 60 sec); 98'C 2 min), each droplet provided a positive or negative fluorescent signal indicating the target gene was present or not present after partitioning. Positive and negative droplets were counted in the QX100 Droplet Reader and the software calculated the concentration of target

gene as copies per microliter. The copy number of each gene was normalized to the housekeeping gene *GAPDH*, which was counted in the same sample.

List of PCR Primers

Gene	ID	RefSeq	Exon boundary
CNTNAP1	Hs00182533_m1	NM_003632.2	18-19
GAPDH	Hs02758991_g1	NM_001256799.1	6..7
MAG	Hs01114387_m1	NM_001199216.1	9..10
MBP	Hs00921945_m1	NM_001025081.1	6..7
NFASC	Hs00391791_m1	NM_001005388.2	11..12
SOX10	Hs00366918_m1	NM_006941.3	3..4
Cntnap1	Mm00489702_m1	NM_016782.2	20..21
Gapdh	Mm99999915_g1	NM_008084.2	2..3
Mag	Mm00487538_m1	NM_010758.2	4..5
Mbp	Mm01266402_m1	nm_001025251.2	3..4
Nfasc	Mm00813922_m1	NM_001160316.1	10..11
Sox10	Mm01300162_m1	NM_011437.1	2..3

Mice

Ts65Dn (RRID: MGI_2178111) and euploid B6EiC3 mice were generated by backcrossing Ts65Dn females to B6EiC3Sn.BLiAF1/J F1 hybrid (B6EiC3) males. The parental generation was obtained from Jackson Laboratory. Quantitative PCR genotyping was performed on genomic DNA extracted from tail tips (Chakrabarti et al., 2007). All procedures regarding the care and death of these animals was approved by the Institutional Animal Care and Use Committee of Boston University School of Medicine, in accordance with the NIH guide for the care and use of laboratory animal. Ts65Dn and euploid littermates at P7, P15, P30 and P60 were anesthetized by ketamine/xylacine cocktail and intracardially perfused with 4% paraformaldehyde (PFA) in 0.1M phosphate buffer saline (PBS, pH 7.4). Perfused brains were removed and fixed in 4% PFA overnight at 4◦C followed by 30% sucrose. All samples were embedded in Tissue-Tek OCT compound (Sakura Finetek), frozen on dry ice and sectioned (16µm) with a Microm HM 560 cryostat (MO BIO Laboratories, Inc).

Immunohistochemistry

All immunohistochemical reactions were performed on 16-µm frozen brain sections. Primary antibodies used were: rabbit anti-Olig2 (1:500, Millipore, RRID: AB_2299035), guinea-pig anti-NG2 (gift from William B. Stallcup, Sanford-Burnham Medical Research Institute, La Jolla, RRID: AB_2314937), mouse anti-RIP (1:50, DSHB), mouse anti-CC1 (CalbioChem), rabbit anti-Caspase3 (1:500, Cell Signaling, RRID: AB_2070042), guinea-pig anti-NF186, rabbit anti-Caspr (1:200, gift from Manzoor Bhat, University of North Carolina at Chapel Hill), mouse anti-MBP (1:1000, Covance, rrid:

AB_2314771) and mouse anti-MAG (1:1000, Millipore, AB_2137847). We used AlexaFluor 488-, AlexaFluor 546- and AlexaFluor 636-conjugated (1:200, Invitrogen) as secondary antibodies. All frozen sections were mounted with Vectashield (Vector Laboratories).

Immunoblotting

Dissected cerebral hemispheres were homogenized in RIPA lysis buffer (Santa Cruz Biotechnology). Proteins were loaded into 4-20% gradient gels. Gels were electrotransferred to a 0.2µm nitrocellulose membrane (Millipore Bioscience Research Reagents). Blots were blocked in 5% milk in TBST and incubated in primary antibodies. Bands were detected with appropriate HRP-conjugated secondary antibodies, reacted with chemiluminescent ECL substrate (Pierce) and imaged. Band intensity was measured using Image J program (National Institute of Health).

Electron Microscopy

8-9 week-old mice were perfused intra-aortically with a warm solution of 2% of paraformaldehyde and 2.5% of glutaraldehyde in phosphate buffer 0.1M at pH 7.2-7.4. Brains were removed and postfixed in the same fixative. To expose the corpus callosum, cerebral hemispheres were separated in the mid-sagittal plane using a razor blade. This was followed by one longitudinal 3mm cut from the midline to each of the cerebral hemispheres. Each thick section was further trimmed into two blocks with which corpus callosum was clearly seen. Sections were rinsed in 0.1M Phosphate buffer for 30 minutes and then incubated in 1% osmium tetroxide during 2-3 hours. Once blocks were osmicated, blocks were dehydrated in an ascending series of alcohols for 2 hours and finally embedded in Araldite. Embedded corpus callosum was sectioned in the transverse plane, such that the nerve fibers were cross-sectioned. Semi-thick (1 µm) sections of the entire corpus callosum were first taken and stained with toluidine blue. For electron microscopy, the block was trimmed so thin sections contained only the corpus callosum. All thin sections were stained with uranyl acetate and lead citrate. All thin sections were mounted on 200 mesh grids, and, after they had been examined to ascertain that the quality of preservation was acceptable, electron micrographs were taken using a JEOL 100S electron microscope. All images were taken in a systematic manner, so electron micrographs were taken approximately in the center of the thin section, and thus focusing on the body of the corpus callosum. 6 images per brain were taken at magnification of 3000x and 8000x. 3000x magnification images were used for counting the myelinated axons, while 8000x magnification images were used to assess g-ratios. To calculate g-ratios, the area of axons and axons plus myelin was measured in electron micrographs by first measuring the circumference of each by hand-tracing tool using Image J, then by calculating areas. A minimum of 3500 axons was counted per animal for assessing numbers of myelinated axons while a minimum of 600 axons was analyzed per animal for assessing g-ratios. Statistical analyses were performed by two-tailed Student's t test analysis. Euploid control, n=3; Ts65Dn, n=3.

Electrophysiology

Mice 2-4 weeks old, were anesthetized and decapitated and the brain was rapidly removed and placed in ice-cold (~ 4°C) cutting artificial cerebrospinal fluid (ACSF) containing (in mM) sucrose 206, KCl 2, $CaCl_2$ 1, NaH_2PO_4 1.25, $MgSO_4$ 2, MgCl-6H_2O 2, NaHCO3 26, d-glucose 10, bubbled with a mixture of 95% O_2/5% CO_2. The mice were then decapitated and the brains placed in a dish of sACSF on ice for blocking. Coronal slices, 400-µm thick, were cut on a Leica VT1200S and transferred to a warmed (~36°C) solution of normal ACSF (nACSF) NaCl 126, KCl 3, $CaCl_2$ 2, NaH_2PO_4 1.25, $MgSO_4$ 2, $NaHCO_3$ 26, d-glucose 10, bubbled with a mixture of 95% O_2/5% CO_2 for 45 minutes. After this recovery period the slices were maintained in the same solution at room temperature for at least 1 hour before recording. All recordings were performed at room temperature (~25 °C). Compound action potentials (CAPs) were evoked by electrical stimulation of the corpus callosum with a bipolar tungsten wire electrode and were recorded with a pulled borosilicate glass pipette (~ 1 MΩ resistance) within the contralateral corpus callosum. Stimulation intensities ranged from 30 to 3000 µA. Input-output curves

were generated by recording the amplitudes of N1 and N2 (see inset Figure 1) as a function of stimulation intensity. The amplitude of each response was taken to be the difference between the corresponding trough and a straight line drawn between the adjacent peaks. Three to five responses were averaged for each measurement. The conduction velocities for myelinated and unmyelinated fibers were calculated as the slope of a straight line fitted through a plot of the distance between the recording and stimulating electrodes versus the response latency (time to N1 or N2 respectively). Refractory periods were measured using a paired pulse protocol where two stimuli were applied with a decreasing time interval (10 to 2 ms) between each pulse. Peak amplitudes and onset latencies were calculated using custom written routines in Igor (WaveMetrics, Lake Oswego, OR). Statistical analysis was performed using SigmaPlot (Systat Software Inc. San Jose, CA) and consisted of repeated measure 2-factor ANOVAs for input-output and refractory period results or a two-tailed Wilcoxon test for conduction velocity data and $p < 0.05$ was assigned for significance.

Image analysis

All fluorescent images were taken on a LSM710 confocal microscope (Carl Zeiss). Three to four brains per genotype were analyzed at each age studied. A minimum of 4 images and up to 6 images per brain were taken for quantitative analysis. 10-μm confocal z-stacks at 40x magnification were analyzed using LSM software to quantify the number of OLIG2+, CC1+, NG2+ and Caspase 3+ cells. 6-μm confocal z-stacks at 63x magnification with zoomX2 were analyzed to quantify the number of nodes using Volocity software (Improvision). For comparative analysis of RIP staining intensity, single plane images were converted to gray-scale. The intensity as the mean gray value obtained from all pixels within a region of interest was quantified using Image J software (National Institutes of Health). All analyses were done blindly to genotype.

Proliferation and Maturation Assays in Oligodendrocyte Progenitor Cultures

Mouse oligodendrocyte precursor cells were isolated by immunopanning through positive selection of cells from postnatal day (P) 7 mouse cerebral cortices that bound to PDGFRA (PDGFRα), as previously described with the exception that Papain treatment was carried out in a 37°C, 5% CO_2 incubator (Emery and Dugas, 2013; Fancy et al., 2011). Cells were plated on poly-D-lysine coated slide wells and allowed to overnight in proliferation conditions with the addition of CNTF, PDGF, and NTF3 (NT-3) (Peprotech) to base medium. For proliferation analysis, cells were allowed to proliferate for an additional 48 hours. For maturation analysis, the media was switched the next morning to contain triiodothyronine (T3; Sigma), but not PDGF or CTNF, and cells were maintained in these conditions for 72 hours in a 5% CO_2 37°C incubator. Cells were fixed for 15 m in 4% paraformaldehyde at room temperature.

Cells left in proliferative conditions were then immunostained for PDGFRA (PDGFRα) and OLIG2. To count the total number of OPCs an image was taken at 10x of the center of 3 slides wells for each sample and OLIG2+ cells were counted using the Cell counter plug in ImageJ (NIH, Bethesday, MD). Cell counts were additionally assessed for contamination form other cells types. No OLIG2/PDGFRA (PDGFRα)–negative cells were observed. Images of MPB/OLIG2 immunostaining were obtained by the same method and the total number OLIG2 cells, in addition to the number of MBP/OLIG2 double positive cells was quantified. To further assess maturation, the complexity of the morphology of MBP cells was categorized into three groups and quantified: simple (i.e. less mature) in which there were fewer than 6 MBP+ processes, complex in which there were more than MBP+ 6 process, and membranous in which a membranous MBP+ lamella without discernible processes extended from the cell body. Student's t-tests were conducted to assess statistical significance (defined as $p < 0.05$) between three experimental replicates.

Statistical Analysis

All data are presented as mean ± SEM, unless otherwise noted. Comparisons of mean differences between groups were made by unpaired two-tailed Student's t-test, except as otherwise noted above

in the extended experimental procedures. A probability level of $p < 0.05$ was considered to be statistically significant.

SUPPLEMENTAL REFERENCES

Emery, B., and Dugas JC. (2013). Purification of oligodendrocyte lineage cells from mouse cortices by immunopanning. Cold Spring Harb. Protoc. *9*,854-868.

Chakrabarti, L., Galdzicki, Z., and Haydar, T.F. (2007). Defects in embryonic neurogenesis and initial synapse formation in the forebrain of the Ts65Dn mouse model of Down syndrome. J. Neurosci. *27*, 11483-11495.

Fancy, S.P., Harrington, E.P., Yuen, T.J., Silbereis, J.C., Zhao, C., Baranzini, S.E., Bruce, C.C., Otero, J.J., Huang, E.J., Nusse, R., et al. (2011). Axin2 as regulatory and therapeutic target in newborn brain injury and remyelination. Nature Neurosci. *14*, 1009-1016.

Herculano-Houzel, S. (2014). The glia/neuron ratio: how it varies uniformly across brain structures and species and what that means for brain physiology and evolution. Glia *62*, 1377-1391.

Kang, H.J., Kawasawa, Y.I., Cheng, F., Zhu, Y., Xu, X., Li, M., Sousa, A.M., Pletikos, M., Meyer, K.A., Sedmak, G., et al. (2011). Spatio-temporal transcriptome of the human brain. Nature *478*, 483-489.

Langfelder, P., and Horvath, S. (2008). WGCNA: an R package for weighted correlation network analysis. BMC Bioinformatics *9*, 559.

Schain, A.J., Hill, R.A., and Grutzendler, J. (2014) Label-free in vivo imaging of myelinated axons in health and disease with spectral confocal reflectance microscopy. Nat. Med. *20*, 443-449.

Zhang, Y., Chen, K., Sloan, S.A., Bennett, M.L., Scholze, A.R., O'Keeffe, S., Phatnani, H.P., Guarnieri, P., Caneda, C., Ruderisch, N., et al. (2014). An RNA-sequencing transcriptome and splicing database of glia, neurons, and vascular cells of the cerebral cortex. J. Neurosci. *34*, 11929-11947.